Received: 8 October 2017 | Revised: 7 January 2018 | Accepted: 24 January 2018

DOI: 10.1002/gj.3175

SPECIAL ISSUE ARTICLE

WILEY

Petrogenesis of rhyolite at Kalatage in the Eastern Tianshan, Northwest China: Evidences from geochemistry, zircon U–Pb geochronology, and Hf isotopes

Xiaohui Sun[1,2] | Yan Luan[1] | Haoshu Tang[2] | Xijuan Tan[1]

[1] School of Earth Science and Resources, Chang'an University, Xi'an, Shaanxi Province, China

[2] State Key Laboratory of Ore Deposit Geochemistry, Institute of Geochemistry, Chinese Academy of Sciences, Guiyang, Guizhou Province, China

Correspondence
Xiaohui Sun, School of Earth Science and Resources, Chang'an University, Xi'an, Shaanxi Province 710054, China.
Email: sunxiaohui@chd.edu.cn

Haoshu Tang, State Key Laboratory of Ore Deposit Geochemistry, Institute of Geochemistry, Chinese Academy of Sciences, Guiyang, Guizhou 550081, China.
Email: tanghaoshu@163.com

Funding information
National Natural Science Foundation of China, Grant/Award Numbers: 41503035, 41672086 and 41603040; Geological Survey of China, Grant/Award Number: 1212011140056; Natural Science Basic Research Plan in Shaanxi Province of China, Grant/Award Numbers: 2017JM4006 and 2016JQ4010; Fundamental Research Funds for the Central Universities, Grant/Award Numbers: 310827151060 and 310827161007

Handling Editor: S. Li

The Central Asian Orogenic Belt was one of the most important sites for juvenile crustal growth during the Phanerozoic worldwide, and Eastern Tianshan, Northwest China, located in southern Central Asian Orogenic Belt, is one of the key areas for unravelling the accretionary processes and continental growth. Zircon U–Pb geochronological, Hf isotopic, and whole-rock geochemical analyses are reported for the Upper Carboniferous Qishan Formation rhyolites from the Kalatage area in the middle of the Harlik–Dananhu arc, Eastern Tianshan, to investigate its petrogenesis and geodynamic setting. Zircon U–Pb ages obtained by laser-ablation inductively coupled mass spectrometry (LA-ICP-MS) indicated that zircon crystallization age of the rhyolite was 299.1 ± 2.1 Ma. The rhyolites are classified as subalkaline and high-K calc-alkaline series with A/CNK values mainly lower than 1.10. The REE patterns exhibit right inclined curves with negative Eu anomalies, and the trace element spider diagrams show depletions in Nb, Ta, and Eu, which is consistent with the geochemical characteristics of the island arc calc-alkaline magma suffered fractional crystallization. In situ zircons Hf isotopic analyses yielded positive initial εHf(t) values ranging from 8.0 to 11.9 and the two-stage Hf isotope crustal model ages (T_{DM}^{C}) of 554 to 807 Ma. It indicated that the rhyolite was derived from remelting of juvenile crust. The geochemical data for the rhyolites indicate that they were probably generated in a suprasubduction zone setting. It is proposed that the North Tianshan oceanic crust subducted northward beneath the Harlik–Dananhu arc during the Late Upper Carboniferous, and the rhyolites were derived from remelting of juvenile crust and generated in a suprasubduction zone setting.

KEYWORDS

crustal growth, Eastern Tianshan, Harlik–Dananhu arc, LA-ICP-MS zircon U–Pb dating, rhyolite, zircon Hf isotope

1 | INTRODUCTION

The Central Asian Orogenic Belt (CAOB) is the largest Phanerozoic orogen in the world and was formed by the amalgamation of various continental blocks, arcs, and accretionary complexes, accompanied by considerable juvenile crustal growth (Ao, Xiao, Han, Mao, & Zhang, 2010; B. Han et al., 1997; B. F. Han, He, Wang, & Hang, 1998; Jahn, Wu, & Chen, 2000; Q. Wang et al., 2007; S. Z. Li et al., 2016; Xiao et al., 2006, 2008; Y. H. Wang et al., 2015) and mineralization (Deng et al., 2016, 2017; Y. J. Chen, 1996, 2000; Y. J. Chen, Pirajno, Wu, Qi, & Xiong, 2012; Y. S. Wu, Chen, & Zhou, 2017; Shen, Pan, Cao, Zhong, & Li, 2017; and references therein). The Tianshan belt occupies the southernmost part of the CAOB and extends over 2,500 km in China, which is a key area for understanding the Palaeozoic tectonic evolution of the CAOB (Y. Y. Zhang et al., 2017). The belt can be geographically divided into the western and eastern segments. The Eastern Tianshan belt occupies a critical tectonic activity position of the southern segment of the CAOB, and it was formed by amalgamation and accretion of continental margin arcs, island arcs, ophiolites, accretionary wedges, turbidites, and overlap sequences situated between the southern active margin of the Siberian Craton to the north and the Tarim Craton to the south from the Ordovician to Early Permian (Mao et al., 2006; Mao et al., 2017; Mao, Fang, Wang, Wang, & Wang, 2010; Mao, Wang, et al., 2014; Mao, Xiao, et al., 2014).

The Kalatage area is located in the middle of the Harlik–Dananhu arc in the Eastern Tianshan belt, and the Ordovician–Jurassic volcanic,

volcaniclastic rocks, and clastic sediments lithologies are widespread in this district (Mao et al., 2010). From Late Ordovician to Early Carboniferous, the North Tianshan ocean subducted northward beneath the Harlik–Dananhu island arc (Mao et al., 2017; Y. Sun et al., 2017). However, the Middle Permian Aerbashayi Formation of the Kalatage area was generated in extensional and/or rift settings (Mao, Wang, et al., 2014; Mao, Xiao, et al., 2014; Zhu et al., 2002). The petrogenesis and tectonic setting of the Upper Carboniferous rocks were poorly understood. Therefore, in this paper, we report geochemical, LA-ICP-MS zircon U–Pb dating, and Lu–Hf isotope data of the Upper Carboniferous Qishan Formation rhyolites from the Kalatage area, Eastern Tianshan, to constrain their petrogenesis and geodynamic setting.

2 | GEOLOGICAL SETTING

The Chinese Tianshan Range is geographically subdivided into the Western Tianshan and Eastern Tianshan with a boundary along the Urumqi–Korla road from west to east (Y. J. Chen et al., 2012). The Eastern Tianshan is a 300-km-wide orogenic collage in the southern Altaids (Xiao, Windley, Allen, & Han, 2013; Xiao, Zhang, Qin, Sun, & Li, 2004) that consists of three tectonic zones: South Tianshan (STS), Central Tianshan (CTS), and North Tianshan (NTS; Figure 1).

The South Tianshan, which is located between the Central Tianshan Arc and the Tarim Craton, comprises various Silurian–Carboniferous rocks, including turbidites, ophiolites (Silurian–Late Carboniferous), cherts, volcaniclastic rocks, mélanges, and Devonian–Early Carboniferous high-pressure metamorphic rocks (Mao, Xiao, et al., 2014; Xiao et al., 2004). The Central Tianshan comprises remnants of the Late Devonian to Carboniferous magmatic arcs, formed by subduction of oceanic crust of the Mansi back-arc basin below the earlier arcs (J. Y. Li, 2004). The North Tianshan is composed of Proterozoic basement and Neoproterozoic to early Palaeozoic magmatic arc rocks of pre-Uralides developed on the margin of the proto-Eurasian continent (X. Chen, Shu, Santosh, & Zhao, 2013).

The North Tianshan tectonic zone comprises the Jueluotage Late Palaeozoic arc, the Kangguer suture zone, and the Palaeozoic Harlik–Dananhu arc from south to north (Xiao et al., 2004). The Ordovician–Carboniferous Harlik–Dananhu arc is located between the Kelameili Palaeozoic suture and the late Carboniferous Kanggur suture zone, and it consists of calc-alkaline mafic–felsic lavas, volcaniclastic tuffs, and flysch sediments (Ma, Shu, & Sun, 1997; Mao, Xiao, et al., 2014; Xiao et al., 2004). The arc-related granitic intrusions with an age of Ordovician to Permian, is especially abundant in the Harlik area (F. W. Chen et al., 2005; G. H. Sun, Li, Gao, & Yang, 2005; Guo, Zhong, & Li, 2006; H. Q. Li et al., 2004; Hou, Tang, Liu, & Wang, 2005; Mao et al., 2010; Mao et al., 2017).

The Kalatage district is located in the middle of the Harlik–Dananhu island arc and adjacent to the Turpan–Hami Basin (Figure 1). It is mainly composed of slightly metamorphosed Palaeozoic mafic to felsic volcanic, volcaniclastic, and sedimentary rocks and is intruded by the Ordovician to Permian granitoids (Figure 2; Mao, Xiao, et al., 2014). Outwards from the Kalatage anticlinal hinge, the rocks are divided into five formations: (a) the Lower Devonian Dananhu Formation consists of biogenic carbonates, clastic sediments, and interbedded volcanic rocks; (b) the Upper Carboniferous Qishan Formation consists of calc-alkaline basaltic and andesitic lavas, tuffs, and clastic sediments; (c) the mid-Permian Aerbashayi Formation is composed of basalts and basaltic andesites interbedded with minor

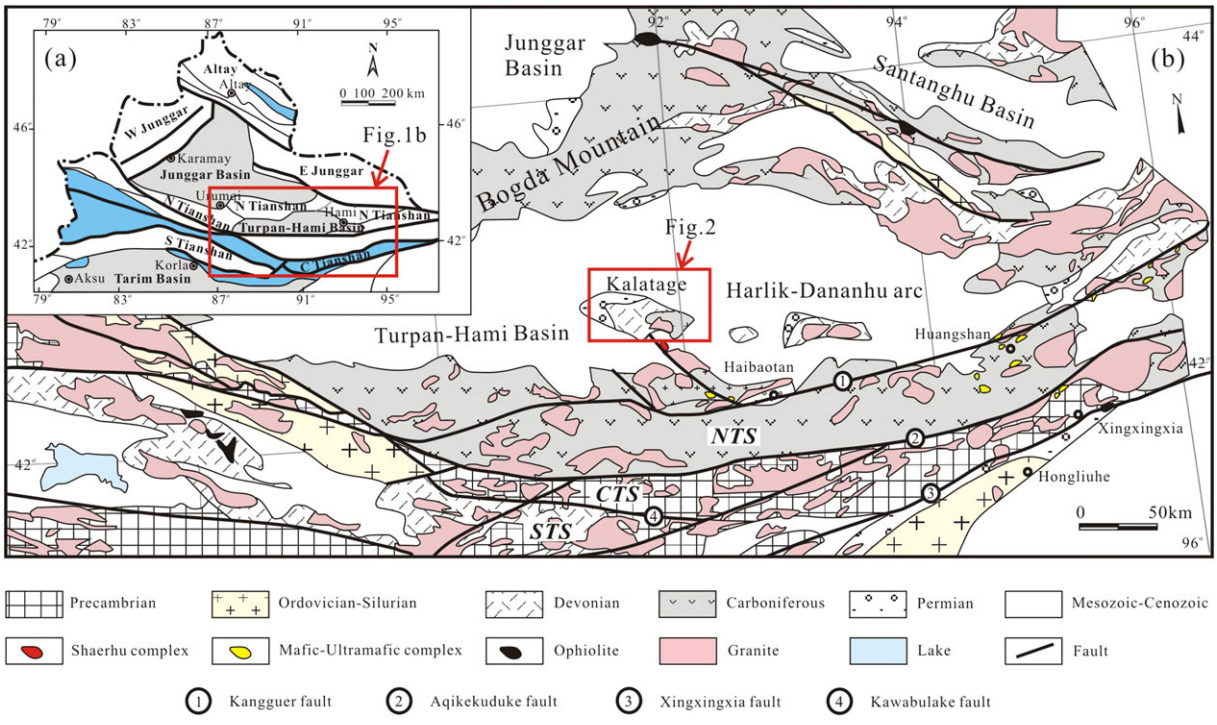

FIGURE 1 (a) Sketch map of geologic units of the Tianshan belt. (b) Schematic geological map of the Eastern Tianshan belt. NTS = North Tianshan; CTS = Central Tianshan; STS = South Tianshan. Modified after Y. J. Chen et al. (2012) and Xiao et al. (2004) [Colour figure can be viewed at wileyonlinelibrary.com]

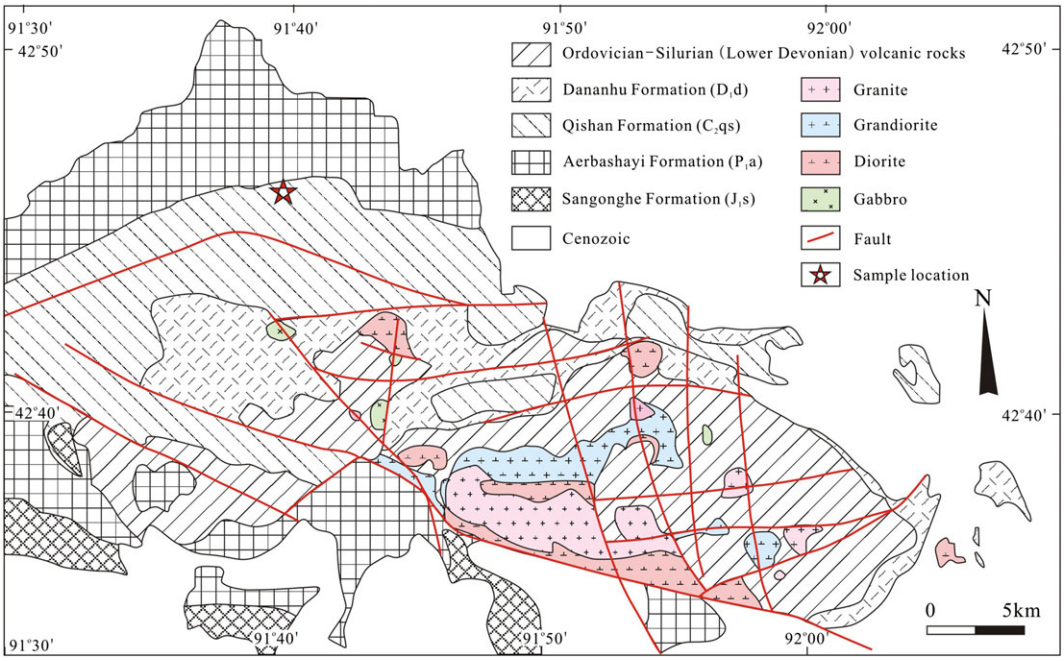

FIGURE 2 Geological map of the Kalatage and adjacent area (modified after Deng et al., 2016, and Mao et al., 2017) [Colour figure can be viewed at wileyonlinelibrary.com]

rhyolites (lower sequence), and tuffs, rhyolites, and dacites (upper sequence); (d) the Upper Permian Kula Formation consists of clastic sediments; and (e) the Lower Jurassic Sangonghe Formation contains black shales, shaly sandstones, sandstones, and coal beds and lies unconformably on all older strata (Mao et al., 2017).

3 | SAMPLING AND PETROLOGY

The rhyolite samples were collected from the Upper Carboniferous Qishan Formation (C_{2qs}). The Qishan Formation is in unconformable relationship with the underlying Lower–Middle Ordovician Qiaganbulake Formation ($O_{1\text{-}2q}$) and the Lower Devonian Dananhu Formation (D_{1d}). And it is unconformably covered by the overlying Middle Permian Kalagang Formation (P_{2k}). The rhyolite is discovered in the Qishan Formation, which originally was named as dacite in the field.

The rhyolites contact with andesite exhibit porphyritic texture, and the content of phenocryst is about 20%. The phenocryst is mainly composed of sanidine, quartz with resorption texture, and biotite with opacitic border texture (Figure 3). The matrix of the rhyolite devitrified to form a few amount of crystallites.

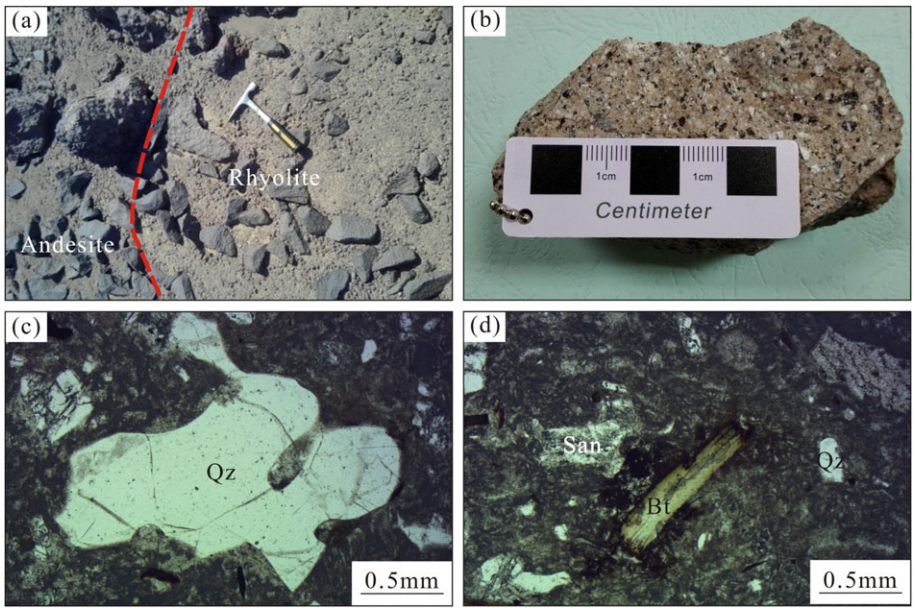

FIGURE 3 Rhyolites from the Kalatage area in the Dananhu arc, NW China. (a) Field photo of rhyolite in contact with andesite (91°39′21″ N, 42°46′09″ E); (b) hand specimen of rhyolite; (c) Photomicrograph of quartz phenocryst exhibiting resorption texture; (d) Photomicrograph of biotite phenocryst possessing opacitic border texture [Colour figure can be viewed at wileyonlinelibrary.com]

TABLE 1 LA-ICP-MS zircon U–Pb isotopic analysis of rhyolites from the Kalatage area in the Dananhu arc, NW China

Spot	Isotope content (ppm)				Ratios						Age (Ma)							
	Pb	Th	U	Th/U	$^{207}Pb/^{206}Pb$	1σ	$^{207}Pb/^{235}U$	1σ	$^{206}Pb/^{238}U$	1σ	$^{207}Pb/^{206}Pb$	1σ	$^{207}Pb/^{235}U$	1σ	$^{206}Pb/^{238}U$	1σ
D6600-1-01	12	89	220	0.41	0.05411	0.00250	0.34842	0.01580	0.04706	0.00075	376	71	304	12	296	5
D6600-1-02	23	215	411	0.52	0.05202	0.00178	0.34326	0.01268	0.04753	0.00066	287	78	300	10	299	4
D6600-1-03	11	83	208	0.40	0.05598	0.00360	0.35581	0.01815	0.04687	0.00086	450	143	309	14	295	5
D6600-1-04	17	136	301	0.45	0.05369	0.00223	0.35195	0.01492	0.04752	0.00062	367	94	306	11	299	4
D6600-1-05	14	126	245	0.52	0.05396	0.00231	0.35411	0.01584	0.04737	0.00060	369	66	308	12	298	4
D6600-1-06	13	128	227	0.56	0.05516	0.00228	0.36249	0.01558	0.04738	0.00063	420	93	314	12	298	4
D6600-1-07	17	138	306	0.45	0.05897	0.00202	0.39005	0.01470	0.04770	0.00071	565	69	334	11	300	4
D6600-1-08	18	148	327	0.45	0.05088	0.00200	0.33055	0.01314	0.04733	0.00068	235	91	290	10	298	4
D6600-1-09	11	75	200	0.37	0.05736	0.00311	0.37231	0.02022	0.04719	0.00071	506	116	321	15	297	4
D6600-1-10	17	145	294	0.49	0.05851	0.00229	0.38566	0.01617	0.04774	0.00080	550	85	331	12	301	5
D6600-1-11	19	164	335	0.49	0.05058	0.00180	0.33379	0.01217	0.04809	0.00073	220	51	292	9	303	4
D6600-1-12	16	143	289	0.49	0.05259	0.00220	0.33942	0.01479	0.04684	0.00068	322	127	297	11	295	4
D6600-1-13	12	66	232	0.29	0.05280	0.00215	0.34600	0.01471	0.04760	0.00061	320	88	302	11	300	4
D6600-1-14	20	146	369	0.40	0.05310	0.00193	0.35464	0.01402	0.04850	0.00070	332	79	308	11	305	4

4 | ANALYTICAL METHODS

4.1 | Major and trace element analysis

The whole-rock major and trace elements were determined at the Laboratory of Mineralization and Dynamics, Chang'an University. Major element compositions were measured using X-ray fluorescence spectrometry (LAB CENTER XRF-1800) on fused glass disks with analytical errors less than 5%. Loss of ignition (LOI) was determined after igniting the sample powder at 1,000 °C for 1 hr. Trace elements (including rare earth elements) analyses were carried out using a Thermo X-7 ICP-MS, and analytical precision was generally better than 10%.

4.2 | Zircon U–Pb dating

Zircons were separated from rhyolite (D6600-1) using conventional heavy liquid and magnetic separation techniques. Representative zircon grains were handpicked under a binocular microscope and then were mounted in an epoxy resin disk and polished to about half of their thickness for analysis. In order to reveal the morphology and internal structure of zircons, cathodoluminescence (CL) images were obtained by using a JSM 6510 scanning electron microscope equipped with a Gatan Mono CL System, at Beijing Geoanalysis Co. Ltd.

Zircon U–Pb dating was conducted by using an Agilent 7700e inductively coupled plasma mass spectrometry (ICP-MS) coupled with a Analyte Excite 193-nm laser at the Laboratory of Mineralization and Dynamics, Chang'an University. Zircon 91500 and NIST610 were used as external calibration standards for zircon U–Pb isotope and trace element analyses, respectively. Zircon isotope ratios and trace elements were calculated using the program ICPMSDataCal 7.2 (Liu et al., 2010). Concordia diagrams and weighted mean calculations were carried out using the Isoplot 3.0 program (Ludwig, 2003).

4.3 | Zircon Hf isotope analysis

Zircon Hf isotope analyses were carried out in situ by using a Nu Plasma HR MC-ICP-MS coupled with a GeoLas 2005 excimer ArF

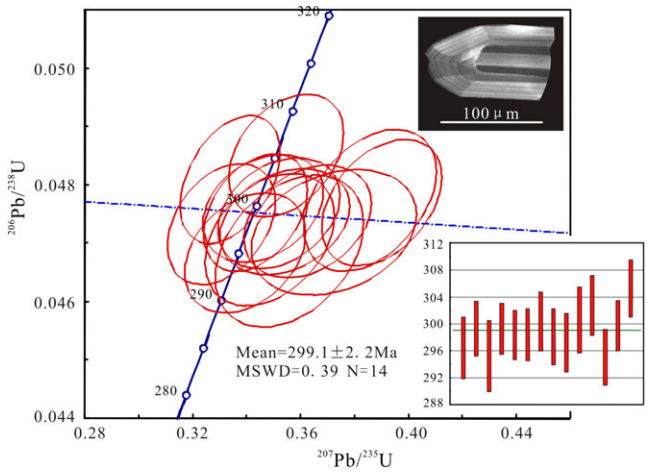

FIGURE 4 Zircon U–Pb concordia diagram, weighted mean $^{206}Pb/^{238}U$ age and representative zircon CL image for the rhyolites [Colour figure can be viewed at wileyonlinelibrary.com]

TABLE 2 Major (%) and trace element (ppm) compositions of rhyolites from the Kalatage area in the Dananhu arc, NW China

Sample no.	D6600-1	D6600-2	D6600-3	D6600-4	D6600-5	D6600-6
SiO_2	72.61	71.68	72.77	72.08	70.55	72.00
TiO_2	0.29	0.28	0.28	0.26	0.34	0.30
Al_2O_3	14.19	13.71	13.80	13.48	13.87	13.53
TFe_2O_3	2.25	2.19	2.13	2.07	2.67	2.24
MnO	0.06	0.06	0.07	0.07	0.07	0.06
MgO	0.60	0.68	0.52	0.69	0.66	0.75
CaO	1.52	1.59	1.62	1.38	1.90	1.57
Na_2O	3.62	3.61	3.67	3.55	3.40	3.22
K_2O	3.73	3.65	3.82	3.90	3.66	3.77
P_2O_5	0.06	0.06	0.06	0.06	0.08	0.06
LOI	2.02	2.33	2.23	3.42	2.48	2.70
Total	100.95	99.84	100.97	100.96	99.68	100.20
A/CNK	1.11	1.07	1.05	1.07	1.07	1.11
A/NK	1.42	1.39	1.36	1.34	1.45	1.44
Li	16.93	13.99	12.22	10.99	9.45	
Be	2.09	2.22	2.27	2.03	2.07	
Sc	3.76	3.49	2.98	2.67	2.39	
V	18.96	27.69	16.57	17.29	17.97	
Cr	9.76	3.37	15.98	6.58	4.59	
Co	28.86	23.55	22.58	20.71	27.03	
Ni	7.84	5.78	4.88	4.51	4.52	
Cu	3.08	3.20	2.63	2.91	2.58	
Zn	47.03	52.46	44.82	40.63	44.11	
Ga	13.79	13.65	12.91	11.94	11.86	
Rb	123.66	119.84	134.00	129.28	105.02	
Sr	178.63	145.29	181.27	274.07	340.36	
Y	26.89	29.65	27.38	25.12	21.66	
Zr	150.49	166.82	145.64	139.83	111.42	
Nb	8.99	9.13	9.35	8.78	8.64	
Mo	1.08	0.66	1.39	0.96	1.15	
Cd	0.17	0.14	0.16	0.14	0.11	
In	0.03	0.03	0.03	0.03	0.03	
Cs	4.13	3.81	6.85	7.27	7.65	
Ba	633.92	526.33	559.39	633.40	569.98	
La	23.37	23.53	23.46	22.16	17.95	
Ce	49.62	49.34	51.09	48.51	40.58	
Pr	5.70	5.84	5.86	5.33	4.52	
Nd	21.21	22.89	21.81	19.90	17.49	
Sm	4.30	4.83	4.29	4.03	3.53	
Eu	0.79	0.88	0.74	0.74	0.72	
Gd	4.32	4.84	4.39	4.02	3.58	
Tb	0.67	0.77	0.70	0.66	0.57	
Dy	4.32	4.82	4.52	4.08	3.71	
Ho	0.89	1.01	0.94	0.90	0.78	
Er	2.97	3.19	3.06	2.85	2.53	
Tm	0.47	0.50	0.49	0.46	0.40	
Yb	3.29	3.57	3.47	3.20	2.83	
Lu	0.50	0.53	0.51	0.51	0.44	
Hf	4.36	4.75	4.56	4.35	3.71	
Ta	0.74	0.73	0.79	0.79	0.75	
Pb	13.30	14.79	17.24	17.12	16.50	
Th	11.56	10.92	13.16	12.62	10.67	
U	3.04	3.11	3.12	3.08	2.86	
∑REE	122.44	126.52	125.33	117.36	99.64	
Eu/Eu*	0.56	0.56	0.52	0.56	0.62	
$(La/Yb)_N$	5.09	4.72	4.85	4.97	4.56	
$(La/Sm)_N$	3.51	3.14	3.53	3.55	3.28	
$(Gd/Yb)_N$	1.09	1.12	1.05	1.04	1.05	

Note. A/CNK = $Al_2O_3/(CaO + Na_2O + K_2O)$ (molar ratios), A/NK = $Al_2O_3/(Na_2O + K_2O)$ (molar ratios), and $Eu/Eu^* = Eu_N/(Sm_N \times Gd_N)^{1/2}$.

laser-ablation system at the State Key Laboratory of Continental Dynamics, Northwest University, Xi'an. The analytical procedures are similar to those described by Yuan et al. (2008). Zircon 91500, Monastery, and GJ-1 were used as external standards in this analysis, and our $^{176}Hf/^{177}Hf$ ratios for the three zircon standards are in good agreement with recommended values.

5 | RESULTS

5.1 | Zircon U–Pb age

The LA-ICP-MS zircon U–Pb age of the rhyolite (D6600-1) was listed in Table 1. Most zircons from the sample are transparent to translucent and occur as euhedral, stubby to prismatic crystals with a length–width ratio of 2:1–4:1. All of the zircon grains show clear oscillatory zoning in the CL image, and their Th/U ratios are 0.29–0.56 with an average of 0.45, demonstrating the typical features of magmatic zircons (Hoskin & Schaltegger, 2003; Y. Wu & Zheng, 2004). Owing to the imprecise ^{207}Pb analyses in Phanerozoic zircons, the more reliable weighted mean $^{206}Pb/^{238}U$ ages of the analysed zircons are adopted here (Compston, Williams, Kirschvink, Zhang, & Ma, 1992). Fourteen zircon grains were analysed for the rhyolite sample D6600-1, and the data are all fall on or near the U–Pb concordia curve, giving $^{206}Pb/^{238}U$ ages from 295 to 305 Ma, with a weighted mean of 299.1 ± 2.2 Ma (Figure 4).

5.2 | Whole-rock geochemistry

The major and trace element data of the rhyolites from the Kalatage area are presented in Table 2. Petrologic investigations have revealed that the samples have been subjected to varying degrees of alteration, which is also confirmed by the relatively high LOI contents, ranging from 2.02 to 3.42 wt.%. The SiO_2 contents of the six rhyolite samples range from 71.68 to 72.08 wt.% with an average of 71.95 wt.%, and Al_2O_3 contents range from 13.53 to 13.80 wt.% with an average of 13.76 wt.%; Na_2O and K_2O contents are in the range of 3.40–3.61 wt.% and 3.65–3.90 wt.%, respectively. All samples are plotted within the rhyolite zone on the total alkali–silica (TAS) diagram (Figure 5a). The A/CNK values range from 1.05 to 1.11, and the A/NK values range from 1.34 to 1.45, demonstrating that they are all peraluminous. All samples are classified as subalkaline (Figure 5a) and high-K calc-alkaline series (Figure 5b).

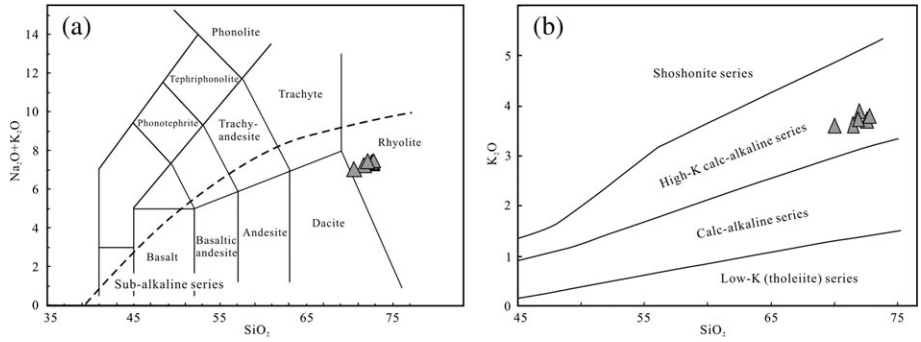

FIGURE 5 Plot of SiO_2 (wt.%) versus $K_2O + Na_2O$ (TAS, wt.%) for the rhyolites (Le Bas, Le Maitre, Streckeisen, & Zanettin, 1986). (b) K_2O–SiO_2 (wt.%) classification diagram (Peccerillo & Taylor, 1976)

In general, the rare earth elements (REE) and the high field strength elements (HFSE) are essentially immobile during alteration (Humphris & Thompson, 1978). Total rare earth element (ΣREE) contents of the rhyolites range from 99.64 to 126.52 ppm. The chondrite-normalized REE distribution patterns exhibit as right inclined curves (Figure 6a), demonstrating light rare earth elements (LREE) relatively enrichment and heavy rare earth elements (HREE) depletion, with $(La/Yb)_N$ ratios ranging from 4.56 to 5.09. The rhyolites possess significantly negative Eu anomalies (Eu/Eu^* = 0.52–0.62) and relative fractionation of LREE ($(La/Sm)_N$ = 3.14–3.55), without significant fractionation of HREEs ($(Gd/Yb)_N$ = 1.04–1.12). The primitive mantle-normalized trace element patterns are characterized by strong enrichment in large ion lithophile elements (LILE) relative to high field strength elements (HFSE), and with pronounced negative Nb and Ta anomalies and positive Rb and Pb anomalies (Figure 6b).

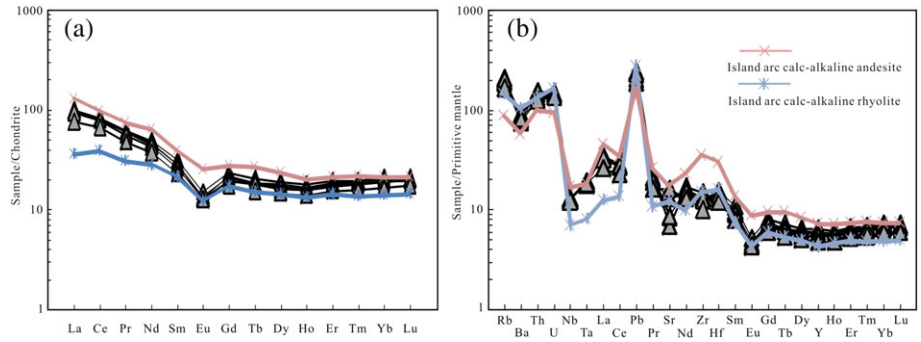

FIGURE 6 (a) Chondrite-normalized REE and (b) primitive mantle-normalized trace element patterns for the rhyolites at the Kalatage area (normalizing values after S. S. Sun & McDonough, 1989). Data of island arc calc-alkaline andesite and rhyolite are from Mao, Wang, et al. (2014) and Muhetare, Nijat, and Wu (2015) [Colour figure can be viewed at wileyonlinelibrary.com]

TABLE 3 Hf isotopic data of zircons from rhyolite in the Kalatage area of the Dananhu arc, NW China

Sample	$^{176}Yb/^{177}Hf$	$^{176}Lu/^{177}Hf$	$^{176}Hf/^{177}Hf$	2σ	t (Ma)	$(^{176}Hf/^{177}Hf)_i$	εHf(0)	εHf(t)	T_{DM1} (Ma)	T_{DM}^C (Ma)	$f_{(Lu/Hf)}$
D6600-1-01.1	0.040435	0.001457	0.282842	0.000020	299	0.282834	2.5	8.8	588	756	−0.96
D6600-1-02.1	0.038367	0.001390	0.282832	0.000022	299	0.282824	2.1	8.4	602	778	−0.96
D6600-1-03.1	0.044556	0.001567	0.282892	0.000021	299	0.282884	4.3	10.5	518	643	−0.95
D6600-1-04.1	0.045919	0.001716	0.282821	0.000022	299	0.282811	1.7	8.0	623	807	−0.95
D6600-1-05.1	0.035319	0.001266	0.282841	0.000019	299	0.282834	2.4	8.8	587	755	−0.96
D6600-1-06.1	0.047748	0.001688	0.282845	0.000027	299	0.282835	2.6	8.8	588	752	−0.95
D6600-1-07.1	0.021666	0.000794	0.282828	0.000022	299	0.282823	2.0	8.4	598	780	−0.98
D6600-1-08.1	0.029459	0.001100	0.282929	0.000022	299	0.282923	5.6	11.9	459	554	−0.97
D6600-1-09.1	0.045298	0.001660	0.282862	0.000020	299	0.282853	3.2	9.4	562	712	−0.95
D6600-1-10.1	0.034219	0.001242	0.282869	0.000023	299	0.282862	3.4	9.8	547	693	−0.96
D6600-1-11.1	0.061176	0.002151	0.282847	0.000024	299	0.282834	2.6	8.8	593	754	−0.94
D6600-1-12.1	0.028365	0.001034	0.282834	0.000022	299	0.282828	2.2	8.6	593	769	−0.97
D6600-1-13.1	0.029467	0.001110	0.282876	0.000020	299	0.282870	3.7	10.0	535	674	−0.97
D6600-1-14.1	0.055919	0.001993	0.282877	0.000029	299	0.282866	3.7	9.9	545	682	−0.94

Note. εHf(t) values are calculated using present-day $(^{176}Lu/^{177}Hf)_{CHUR}$ = 0.0332 and $(^{176}Hf/^{177}Hf)_{CHUR}$ = 0.282772 (Blichert-Toft & Albarède, 1997). T_{DM}^C values are calculated using present-day $(^{176}Lu/^{177}Hf)_{DM}$ = 0.0384 and $(^{176}Hf/^{177}Hf)_{DM}$ = 0.28325. $^{176}Hf/^{177}Hf$ value for the average continental crust is 0.015 (Griffin et al., 2000). The decay constant of ^{176}Lu is 1.867×10^{-11}/a (Söderlund, Patchett, Vervoort, & Isachsen, 2004).

5.3 | Zircon Hf isotopic compositions

Zircon Lu–Hf isotope analysis was performed for the rhyolites at 14 test points that are located in the same magmatic oscillatory zone where the U–Pb dating was performed. We calculated the εHf(t) values and two-stage Hf isotope model ages (T_{DM}^{C}) using the weighted zircon $^{206}Pb/^{238}U$ age for the rhyolites. The Lu–Hf isotope compositions and calculation results are listed in Table 3. All the measured zircon grains had relatively homogeneous Hf isotopic composition ($^{176}Hf/^{177}Hf$ = 0.282821–0.282929), corresponding to the two-stage Hf isotope crustal model ages (T_{DM}^{C}) of 554–807 Ma. In the εHf(t)–U/Pb age diagram, zircons from the Qishan Formation rhyolite showed a spread of εHf(t) values between the chondritic uniform reservoir (CHUR) reference line and the depleted mantle evolution line, ranging from 8.0 to 11.9, which are different from those of the Early Permian Bogda rhyolite from bimodal rock series generated in a postcollisional setting (Figure 7).

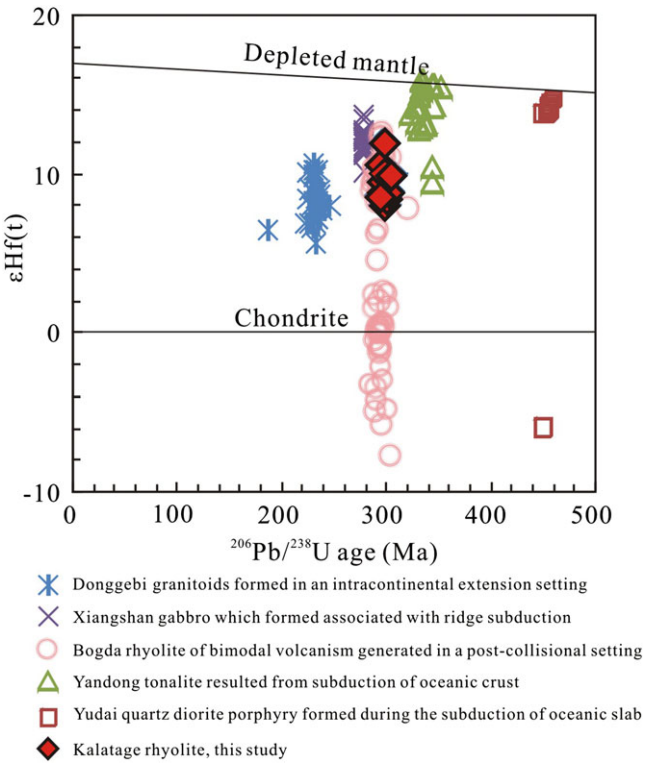

FIGURE 7 Diagram of εHf(t) versus U–Pb ages of the Eastern Tianshan igneous rocks. Data for the Donggebi granitoids (after F. F. Zhang, Wang, Liu, & Wang, 2015), Xingshan gabbro (after C. M. Han et al., 2010), Bogda rhyolite (after X. Chen, Shu, & Santosh, 2011), Yandong tonalite (after Y. H. Wang et al., 2015), and Yudai quartz dioritic porphyry (after Y. Sun et al., 2017) [Colour figure can be viewed at wileyonlinelibrary.com]

6 | DISCUSSION

6.1 | Petrogenesis

Rock type of magmatic rocks is closely related with the geodynamic process. The rhyolites from the Qishan Formation in the Kalatage area display that the A/CNK values are lower (<1.11). And the lack of typical peraluminous minerals (e.g., cordierite, andalusite, and garnet) or alkaline mafic minerals (e.g., aegirine, riebeckite, and alkali amphibole) indicates that the rhyolites belong to I-type granitoid series (Chappell & White, 1992; X. Chen et al., 2013). The right inclined curve REE patterns with LREE enrichment and HREE depletion are consistent with the geochemical characteristics of island arc calc-alkaline magmas (Peccerillo & Taylor, 1976; Schmidberger & Hegner, 1999). The calc-alkaline rhyolites are characterized by depletion of Nb and Ta relative to Th and the LREE (Figure 6b); these geochemical features are also characteristic of subduction-related magmatism (Pearce & Peate, 1995; Sajona, Maury, Bellon, Cotten, & Defant, 1996). In the Rb/Y versus Nb/Y diagram (Figure 8a), the Kalatage rhyolite samples plot close to lower crustal compositions. Moreover, the rhyolites plot near subduction zone compositions in the Th/Yb versus Ta/Yb diagram (Figure 8b).

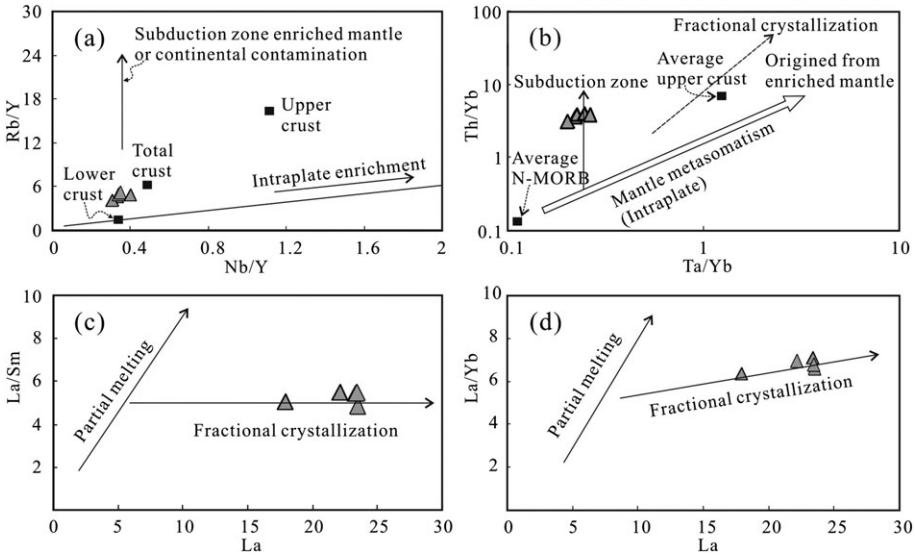

FIGURE 8 Diagram of Diagram of (a) Rb/Y versus Nb/Y, (b) Th/Yb versus Ta/Yb, (c) La/Sm versus La and (d) La/Yb versus La for rhyolites from the Kalatage area of the Eastern Tianshan

The Qishan Formation rhyolites exhibit relatively low contents of MgO, which is consistent with the differentiated nature of the magma (Mao, Xiao, et al., 2014). The fractionation trends in the magmatic rocks are also clearly indicated by the rhyolites with the striking depletions in Ba, Sr, and Eu in the spider diagrams. For instance, the highly negative Eu depletion requires magma to have undergone extensive fractionation of plagioclase. In the La/Sm versus La and La/Yb versus La diagrams, the rhyolites also mainly show a fractional crystallization trend (Figure 8c,d). All these features indicate that the rocks underwent extensive magmatic differentiation.

In general, the acid rocks with low εHf(t) values and older model ages indicate that they were formed by palaeo-crustal anatexis or remelting, whereas the high εHf(t) values and younger model ages were thought to be formed by the recycling of juvenile crust or the invasion of slab-derived materials in the continental crust (Allègre & Othman, 1980; Jahn, Wu, & Hong, 2000). As for this study, the zircon U–Pb age of 299.1 ± 2.2 Ma with the positive εHf(t) values (8.0 to 11.9) and relatively young Hf isotope crustal model ages (T_{DM}^{C}) of 554–807 Ma indicates that the rhyolites were derived from remelting of juvenile crust, and the geochemical characteristics indicate that the melt suffered magmatic differentiation.

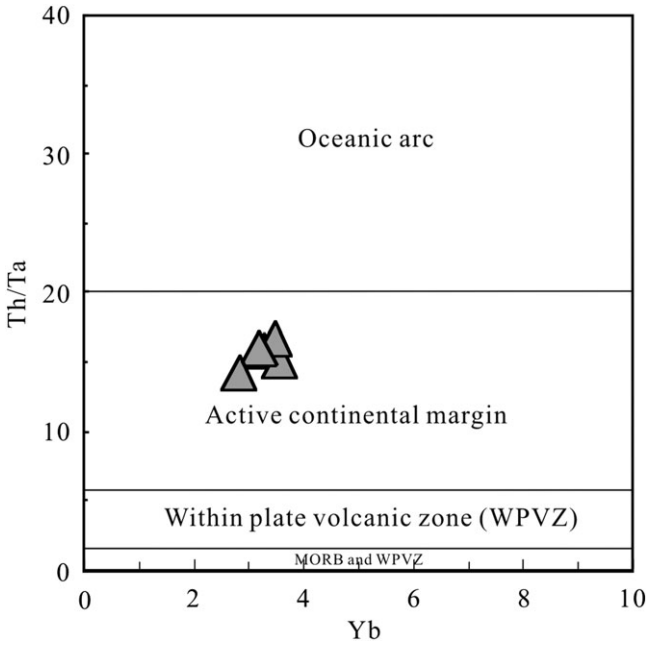

FIGURE 9 Diagram Yb versus Th/La for rhyolites from the Kalatage area of the Eastern Tianshan (after Gorton & Schandl, 2000)

6.2 | Tectonic implication

The Harlik–Dananhu arc is located between the Kelameili Palaeozoic suture and the Late Carboniferous Kanggur suture zone. Previous studies about the Palaeozoic tectonic evolution of the Harlik–Dananhu arc, has gotten a broad consensus that the arc accretion was from north to south (G. H. Sun et al., 2005; H. R. Zhang, Wei, Li, Du, & Cai, 2010; L. C. Zhang, Qin, Ying, Xia, & Xu, 2004; L. C. Zhang, Xiao, Qin, & Zhang, 2006; W. M. Li, Ren, Yang, Li, & Chen, 2002; Xiao et al., 2010; X. Chen et al., 2013; Y. H. Wang et al., 2015).

With regard to the Kalatage area that is located in the middle of the Harlik–Dananhu arc in the Eastern Tianshan belt, it is mainly composed of Ordovician to Permian rocks. Previous studies were focused on revealing the tectonic evolution from Late Ordovician to Permian in this district and followed as (a) in the Late Ordovician, the Kangguer Ocean slab that was subducted northward beneath the Dananhu island

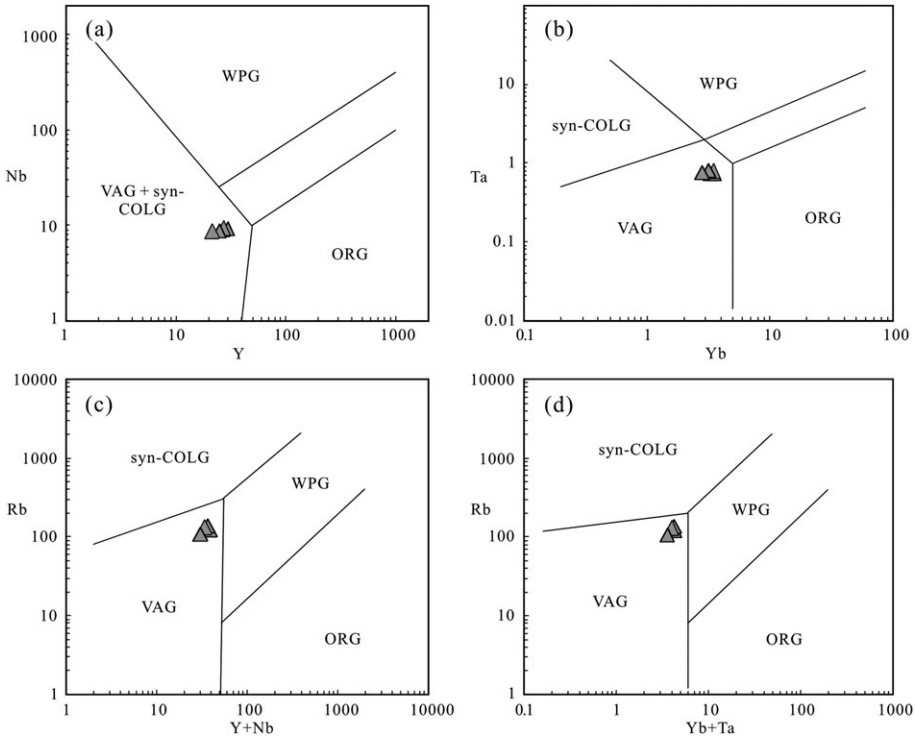

FIGURE 10 Discrimination diagrams of tectonic setting of rhyolites from the Kalatage area of the Eastern Tianshan (after Pearce, Harris, & Tindle, 1984). Syn-COLG = syn-collision granites; VAG = volcanic arc granites; WPG = within-plate granites; ORG = ocean ridge granites

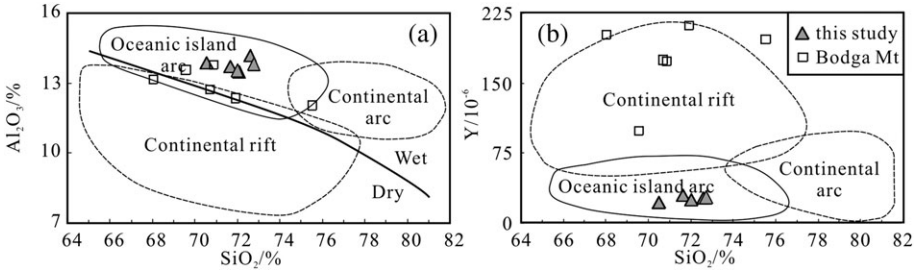

FIGURE 11 The content of major and trace elements of rhyolites from different tectonic settings (after Ayalew & Ishiwatari, 2011) and rhyolite from Bogda belt after X. Chen et al. (2011), which is of bimodal rock series generated in a postcollisional setting

arc to form the Yudai porphyry Cu (Au, Mo) mineralization in the Kalatage district (Y. Sun et al., 2017); (b) in the early Carboniferous (334–322 Ma), more subducted oceanic crust melted in the North Tianshan suprasubduction zone, generating a considerable volume of arc-related volcanic rocks and granitic intrusions in the Harlik–Dananhu arc (Mao et al., 2017); (c) in the early Permian, oblique subduction in the southern Altaids gave rise to strike-slip extensional faults, which controlled the emplacement of large volumes of mantle-derived melts to form the Shaerhu alkaline complex (age of 286 Ma) in the Kalatage area, and the Early Permian Shaerhu alkaline complex was generated in a suprasubduction zone setting (Mao, Xiao, et al., 2014); and (d) in the Middle Permian, the bimodal (basic–acidic) volcanic rocks of the Aerbashayi Formation were emplaced in extensional and/or rift settings (Zhu et al., 2002). From the above discussion, it is showed that the Upper Carboniferous rocks were poorly understood in the Kalatage area.

Based on the LA-ICP-MS zircon U–Pb dating data obtained in this study, it indicates that the rhyolites from the Qishan Formation have occurred around 300 Ma in the Kalatage area, Eastern Tianshan. The obvious negative Nb and Ta anomalies and positive Th and U anomalies, and the enrichment of LREEs with negative Eu anomalies of the rhyolites, indicate that these rhyolites were formed in a suprasubduction zone environment. In the Th/Ta versus Yb discrimination diagram, the rhyolites indicate an active continental margin affinity (Figure 9). Furthermore, the samples of rhyolites all fall within the volcanic arc field in the tectonic discrimination diagrams of Y–Nb, Yb–Ta, (Y + Nb)–Rb, and (Y + Ta)–Rb, suggesting of a subduction setting (Figure 10). As in Figure 11, the rhyolites showed high contents in Al_2O_3 but low contents in Y, which is different from those of rhyolite generated in a postcollisional setting of Bogda belt, whereas consistent with the element characteristics of ocean island arc. Consequently, we prefer to hold that it was subduction-dominated setting related to the northward subduction of the North Tianshan oceanic crust rather than a postcollisional environment during the Late Upper Carboniferous in the Kalatage area, Eastern Tianshan. In summary, the Qishan Formation rhyolites in the Kalatage area had undergone extensive magmatic differentiation. The rocks were derived from remelting of juvenile crust and generated in a suprasubduction zone setting.

7 | CONCLUSIONS

1. Zircon LA-ICP-MS U–Pb dating for the Qishan Formation rhyolites in the Kalatage area, Eastern Tianshan of NW China, yielded crystallization age of 299.1 ± 2.1 Ma, indicating that it erupted during the Late Upper Carboniferous.
2. The rhyolites are high-K calc-alkaline rocks. The εHf(t) values of 8.0 to 11.9 and the two-stage Hf isotope crustal model ages (T_{DM}^{C}) of 554 to 807 Ma indicate that it was derived from remelting of juvenile crust.
3. The rhyolites of the Qishan Formation were most likely generated in a suprasubduction zone setting, which resulted from northward subduction of the North Tianshan oceanic crust beneath the Harlik–Dananhu arc during the Late Upper Carboniferous.

ACKNOWLEDGEMENTS

This work was jointly supported financially by the National Natural Science Foundation of China (Grants 41503035, 41672086, and 41603040), Geological Survey of China (1212011140056), the Natural Science Basic Research Plan in Shaanxi Province of China (Grants 2017JM4006 and 2016JQ4010), and Fundamental Research Funds for the Central Universities (310827151060 and 310827161007). We would like to thank Prof. Gaoxue Yang, Mr. Yong Liu, and Lei Zhang for their help in data collection and filed investigation. We also gratefully acknowledge Dr. Zhuming Wang and Jinhua Du from the Laboratory of Mineralization and Dynamics, Chang'an University, for their help in major and trace element analysis, and Dr. Zhian Bao from State Key Laboratory of Continental Dynamics, Northwest University, for zircon Hf isotope analysis. We are grateful to Prof. Sanzhong Li and two anonymous reviewers for their careful corrections, relevant comments, and constructive suggestions to the manuscript.

ORCID

Xiaohui Sun http://orcid.org/0000-0002-0018-8002
Yan Luan http://orcid.org/0000-0002-9430-4333

REFERENCES

Allègre, C. J., & Othman, D. B. (1980). Nd-Sr isotopic relationship in granitoid rocks and continental crust development: A chemical approach to orogenesis. *Nature*, *286*, 335–342.

Ao, S. J., Xiao, W. J., Han, C. M., Mao, Q. G., & Zhang, J. E. (2010). Geochronology and geochemistry of Early Permian mafic–ultramafic complexes in the Beishan area, Xinjiang, NW China: Implications for late Paleozoic tectonic evolution of the southern Altaids. *Gondwana Research*, *18*, 466–478.

Ayalew, D., & Ishiwatari, A. (2011). Comparison of rhyolites from continental rift, continental arc and oceanic island arc: Implication for the mechanism of silicic magma generation. *Island Arc*, *20*(1), 78–93.

Blichert-Toft, J., & Albarède, F. (1997). The Lu-Hf isotope geochemistry of chondrites and the evolution of the mantle-crust system. *Earth and Planetary Science Letters*, *148*, 243–258.

Chappell, B. W., & White, A. J. R. (1992). I-and S-type granites in the Lachlan Fold Belt. *Geological Society of America Special Papers*, *272*, 1–26.

Chen, F. W., Li, H. Q., Chen, Y. C., Wang, D. H., Wang, J. L., Liu, D. Q., … Zhou, R. H. (2005). Zircon SHRIMP U-Pb dating and its geological significance of mineralization in Tuwu-Yandong porphyry copper mine, East Tian Shan Mountain. *Acta Geologica Sinica*, *79*, 256–261. (in Chinese with English abstract)

Chen, X., Shu, L., & Santosh, M. (2011). Late Paleozoic post-collisional magmatism in the Eastern Tianshan Belt, Northwest China: New insights from geochemistry, geochronology and petrology of bimodal volcanic rocks. *Lithos*, *127*, 581–598.

Chen, X., Shu, L., Santosh, M., & Zhao, X. (2013). Island arc-type bimodal magmatism in the eastern Tianshan Belt, Northwest China: Geochemistry, zircon U-Pb geochronology and implications for the Paleozoic crustal evolution in Central Asia. *Lithos*, *168*, 48–66.

Chen, Y. J. (1996). Mineralization during collisional orogenesis and its control of the distribution of gold deposits in Junggar Mountains, Xinjiang, China. *Acta Geologica Sinica*, *71*, 69–79.

Chen, Y. J. (2000). Progress in the study of Central Asia-type orogenesis—Metallogenesis in Northwest China. *Geological Journal of China Universities*, *6*, 17–22. (in Chinese with English abstract)

Chen, Y. J., Pirajno, F., Wu, G., Qi, J. P., & Xiong, X. L. (2012). Epithermal deposits in North Xinjiang, NW China. *International Journal of Earth Sciences*, *101*, 889–917.

Compston, W., Williams, I. S., Kirschvink, J. L., Zhang, Z. C., & Ma, G. G. (1992). Zircon U-Pb ages for the Early Cambrian time-scale. *Journal of the Geological Society of London*, *149*, 171–184.

Deng, X. H., Chen, Y. J., Santosh, M., Wang, J. B., Li, C., Yue, S. W., … Qu, X. (2017). U-Pb zircon, Re-Os molybdenite geochronology and Rb-Sr geochemistry from the Xiaobaishitou W (-Mo) deposit: Implications for Triassic tectonic setting in eastern Tianshan, NW China. *Ore Geology Reviews*, *80*, 332–351.

Deng, X. H., Wang, J. B., Pirajno, F., Wang, Y. W., Li, Y. C., Li, C., … Chen, Y. J. (2016). Re-Os dating of chalcopyrite from selected mineral deposits in the Kalatag district in the eastern Tianshan Orogen, China. *Ore Geology Reviews*, *77*, 72–81.

Gorton, M. P., & Schandl, E. S. (2000). From continents to island arcs: A geochemical index of tectonic setting for arc-related and within-plate felsic to intermediate volcanic rocks. *The Canadian Mineralogist*, *38*, 1065–1073.

Griffin, W. L., Pearson, N. J., Belousova, E., Jackson, S. E., van Achterbergh, E., O'Reilly, S. Y., & Shee, S. R. (2000). The Hf isotope composition of cratonic mantle: LAM-MC-ICPMS analysis of zircon megacrysts in kimberlites. *Geochimica et Cosmochimica Acta*, *64*, 133–147.

Guo, H. C., Zhong, L., & Li, L. Q. (2006). Zircon SHRIMP U-Pb dating of quartz diorite in the Koumenzi area, Karlik Mountains, East Tianshan, Xinjiang, China, and its geological significance. *Geological Bulletin of China*, *25*, 928–931. (in Chinese with English abstract)

Han, B., Wang, S., Jahn, B.-M., Hong, D., Kagami, H., & Sun, Y. (1997). Depleted mantle so for the Ulungur River A-type granites from North Xinjiang, China: Geochemistry Nd-Sr isotopic evidence, and implications for the Phanerozoic crustal growth. *Chemical Geology*, *138*, 135–159.

Han, B. F., He, G. Q., Wang, S. G., & Hang, D. W. (1998). Post-collisional mantle-derived magmatism and vertical growth of the continental crust in north Xinjiang. *Geological Review*, *44*, 396–406. (in Chinese with English abstract)

Han, C. M., Xiao, W. J., Zhao, G. C., Ao, S. J., Zhang, J., Qu, W. J., & Du, A. D. (2010). In-situ U–Pb, Hf and Re–Os isotopic analyses of the Xiangshan Ni–Cu–Co deposit in Eastern Tianshan (Xinjiang), Central Asia Orogenic Belt: Constraints on the timing and genesis of the mineralization. *Lithos*, *120*(3), 547–562.

Hoskin, P. W., & Schaltegger, U. (2003). The composition of zircon and igneous and metamorphic petrogenesis. *Reviews in Mineralogy and Geochemistry*, *53*(1), 27–62.

Hou, G. S., Tang, H. F., Liu, C. Q., & Wang, Y. B. (2005). Geochronological and geochemical study on the wallrock of Tuwu-Yandong porphyry copper deposits, eastern Tianshan mountains. *Acta Petrologica Sinica*, *21*, 1729–1736. (in Chinese with English abstract)

Humphris, S. E., & Thompson, G. (1978). Hydrothermal alteration of oceanic basalts by seawater. *Geochimica et Cosmochimica Acta*, *42*, 107–125.

Jahn, B. M., Wu, F. Y., & Chen, B. (2000). Granitoids of the Central Asian Orogenic Belt and continental growth in the Phanerozoic. *Transactions of the Royal Society of Edinburgh: Earth Sciences*, *91*, 181–193.

Jahn, B. M., Wu, F. Y., & Hong, D. W. (2000). Important crustal growth in the Phanerozoic: Isotopic evidence of granitoids from east-central Asia. *Journal of Earth System Science*, *109*, 5–20.

Le Bas, M. J., Le Maitre, R. W., Streckeisen, A., & Zanettin, B. (1986). A chemical classification of volcanic rocks based on the total alkali–silica diagram. *Journal of Petrology*, *27*, 745–750.

Li, H. Q., Chen, F. W., Lu, Y. F., Yang, H. M., Guo, J., & Mei, Y. P. (2004). Zircon SHRIMP U-Pb age and strontium isotopes of mineralized granitoids in the Sanchakou copper polymetallic deposit, East Tianshan Mountains. *Acta Geoscientia Sinica*, *25*, 191–195. (in Chinese with English abstract)

Li, J. Y. (2004). Late Neoproterozoic and Paleozoic tectonic framework and evolution of eastern Xinjiang, NW China. *Geological Review*, *50*, 304–322. (in Chinese with English abstract)

Li, S. Z., Yang, Z., Zhao, S. J., Li, M. Y., Suo, Y. H., Guo, L. L., … Mu, D. L. (2016). Global Early Paleozoic orogens (II): Subduction-accretionary-type orogeny. *Journal of Jilin University (Earth Science Edition)*, *46*, 968–1004.

Li, W. M., Ren, B. C., Yang, X. K., Li, Y. Z., & Chen, Q. (2002). The intermediate–acid intrusive magmatism and its geodynamic significance in eastern Tianshan region. *Northwestern Geology*, *4*, 41–64. (in Chinese with English abstract)

Liu, Y. S., Hu, Z. C., Zong, K. Q., Gao, C. G., Gao, S., Xu, J., & Chen, H. H. (2010). Reappraisement and refinement of zircon U-Pb isotope and trace element analyses by LA-ICP-MS. *Chinese Science Bulletin*, *55*, 1535–1546.

Ludwig, K. R. (2003). *ISOPLOT 3.00: A geochronological toolkit for Microsoft excel*. Berkeley: Berkeley Geochronology Center.

Ma, R. S., Shu, L. S., & Sun, J. Q. (1997). *Tectonic evolution and metallization in the eastern Tianshan Belt, China*. (p. 202). Beijing: Geological Publish House. (in Chinese with English abstract)

Mao, Q. G., Fang, T. H., Wang, J. B., Wang, S. L., & Wang, N. (2010). The geochronology studies of the early Paleozoic Honghai massive sulfide deposits and its geological significance, Kalatage belt in eastern Tianshan Mountain, Xinjiang, northwest China. *Acta Petrologica Sinica*, *26*, 3017–3026. (in Chinese with English abstract)

Mao, Q. G., Wang, J. B., Xiao, W. J., Fang, T. H., Wang, N., & Yu, M. J. (2014). The discovery of Low-Carboniferous arc volcanic rocks and its tectonic significance at the Kalatage area in the Central Tianshan, Eastern Tianshan Mountains, Xinjiang, NW China. *Acta Geologica Sinica*, *88*(10), 1790–1799.

Mao, Q. G., Xiao, W. J., Fang, T. H., Windley, B. F., Sun, M., Ao, S. J., … Huang, X. (2014). Geochronology, geochemistry and petrogenesis of Early Permian alkaline magmatism in the Eastern Tianshan: Implications for tectonics of the Southern Altaids. *Lithos*, *190*, 37–51.

Mao, Q. G., Xiao, W. J., Han, C. M., Sun, M., Yuan, C., Yan, Z., … Zhang, J. E. (2006). Zircon U-Pb age and the geochemistry of the Baishiquan mafic-ultramafic complex in the eastern Tianshan, Xinjiang: Constraints on the closure of the Paleo-Asian Ocean. *Acta Petrologica Sinica*, *22*, 153–162. (in Chinese with English abstract)

Mao, Q. G., Yu, M. J., Xiao, W. J., Windley, B. F., Li, Y. C., Wei, X. F., … Lü, X. (2017). Skarn-mineralized porphyry adakites in the Harlik arc at Kalatage, E. Tianshan (NW China): Slab melting in the Devonian-early

Carboniferous in the southern Central Asian Orogenic Belt. *Journal of Asian Earth Sciences*. https://doi.org/10.1016/j.jseaes.2017.03.021

Muhetare, Z., Nijat, A., & Wu, Z. (2015). Geochemical characteristics of the volcanics from the southern Jueluotage area and their constraints on the tectonic evolution of Paleo-Asian Ocean. *Earth Science Frontiers*, *22*(1), 238–250.

Pearce, J. A., Harris, N. B. W., & Tindle, A. G. (1984). Trace element discrimination diagrams for the tectonic interpretation of granitic rocks. *Journal of Petrology*, *25*, 956–983.

Pearce, J. A., & Peate, D. W. (1995). Tectonic implications of the composition of volcanic arc magmas. *Annual Review of Earth and Planetary Sciences*, *23*, 251–285.

Peccerillo, A., & Taylor, S. R. (1976). Geochemistry of Eocene calc-alkaline volcanic rocks from the Kastamonu area, northern Turkey. *Contributions to Mineralogy and Petrology*, *58*, 63–81.

Sajona, F. G., Maury, R. C., Bellon, H., Cotten, J., & Defant, M. (1996). High field strength element enrichment of Pliocene–Pleistocene island-arc basalts, Zamboanga Peninsula, Western Mindanao (Philippines). *Journal of Petrology*, *37*, 693–726.

Schmidberger, S. S., & Hegner, E. (1999). Geochemistry and isotope systematics of calc-alkaline volcanic rocks from the Saar-Nahe basin (SW Germany)—Implications for Late-Variscan orogenic development. *Contributions to Mineralogy and Petrology*, *135*(4), 373–385.

Shen, P., Pan, H., Cao, C., Zhong, S., & Li, C. (2017). The formation of the Suyunhe large porphyry Mo deposit in the west Junggar terrain, NW China: Zircon U-Pb age, geochemistry and Sr-Nd-Hf isotopic results. *Ore Geology Reviews*, *81*, 808–828.

Söderlund, U., Patchett, P. J., Vervoort, J. D., & Isachsen, C. E. (2004). The ^{176}Lu decay constant determined by Lu-Hf and U-Pb isotope systematics of Precambrian mafic intrusions. *Earth and Planetary Science Letters*, *219*, 311–324.

Sun, G. H., Li, J. Y., Gao, L. M., & Yang, T. N. (2005). Zircon SHRIMP U-Pb age of a dioritic pluton in the Harlik mountain, eastern Xinjiang, and its tectonic implication. *Geological Review*, *51*, 463–469. (in Chinese with English abstract)

Sun, S. S., & McDonough, W. F. (1989). Chemical and isotopic systematics of oceanic basalts: Implications for mantle composition and processes. In A. D. Saunders, & M. J. Norry (Eds.), *Magmatism in the ocean basin Geological Society special publication vol. 42* (pp. 313–345). London: Blackwell Scientific Publications.

Sun, Y., Wang, J. B., Li, Y. C., Wang, Y. W., Yu, M. J., Long, L. L., … Chen, L. (2017). Recognition of Late Ordovician Yudai porphyry Cu (Au, Mo) mineralization in the Kalatag district, Eastern Tianshan terrane, NW China: Constraints from geology, geochronology, and petrology. *Ore Geology Reviews*. https://doi.org/10.1016/j.oregeorev.2017.07.011

Wang, Q., Wyman, D. A., Zhao, Z. H., Xu, J. F., Zheng, H. B., Xiong, X. L., … Chu, Z. Y. (2007). Petrogenesis of Carboniferous adakites and Nb-enriched arc basalts in the Alataw area, northern Tianshan range (western China): Implications for Phanerozoic crustal growth in the Central Asia orogenic belt. *Chemical Geology*, *236*, 42–64.

Wang, Y. H., Xue, C. J., Wang, J. P., Peng, R. M., Yang, J. T., Zhang, F. F., … Zhao, Y. J. (2015). Petrogenesis of magmatism in the Yandong region of Eastern Tianshan, Xinjiang: Geochemical, geochronological, and Hf isotope constraints. *International Geology Review*, *57*(9–10), 1130–1151.

Wu, Y., & Zheng, Y. (2004). Genesis of zircon and its constraints on interpretation of U-Pb age. *Chinese Science Bulletin*, *49*(15), 1554–1569.

Wu, Y. S., Chen, Y. J., & Zhou, K. F. (2017). Mo deposits in Northwest China: Geology, geochemistry, geochronology and tectonic setting. *Ore Geology Reviews*, *81*, 641–671.

Xiao, W. J., Han, C. M., Yuan, C., Chen, H. L., Sun, M., Lin, S. F., … Li, J. L. (2006). The unique Carboniferous-Permian tectonic-metallogenic framework of Northern Xinjiang (NW China): Constraints for the tectonics of the southern Paleoasian Domain. *Acta Petrologica Sinica*, *22*, 1362–1376. (in Chinese with English abstract)

Xiao, W. J., Han, C. M., Yuan, C., Sun, M., Lin, S. F., Chen, H. L., … Sun, S. (2008). Middle Cambrian to Permian subduction-related accretionary orogenesis of Northern Xinjiang, NW China: Implications for the tectonic evolution of Central Asia. *Journal of Asian Earth Sciences*, *32*, 102–117.

Xiao, W. J., Mao, Q. G., Windley, B. F., Qu, J. F., Zhang, J. E., Ao, S. J., … Li, J. L. (2010). Paleozoic multiple accretionary and collisional processes of the Beishan orogenic collage. *American Journal of Science*, *310*, 1553–1594.

Xiao, W. J., Windley, B. F., Allen, M. B., & Han, C. M. (2013). Paleozoic multiple accretionary and collisional tectonics of the Chinese Tianshan orogenic collage. *Gondwana Research*, *23*, 1316–1341.

Xiao, W. J., Zhang, L. C., Qin, K. Z., Sun, S., & Li, J. L. (2004). Paleozoic accretionary and collisional tectonics of the Eastern Tianshan (China): Implications for the continental growth of central Asia. *American Journal of Science*, *304*, 370–395.

Yuan, H. L., Gao, S., Dai, M. N., Zong, C. L., Günther, D., Fontaine, G. H., … Diwu, C. R. (2008). Simultaneous determinations of U–Pb age, Hf isotopes and trace element compositions of zircon by excimer laser-ablation quadrupole and multiple-collector ICP-MS. *Chemical Geology*, *247*, 100–118.

Zhang, F. F., Wang, Y. H., Liu, J. J., & Wang, J. P. (2015). Zircon U–Pb and molybdenite Re–Os geochronology, Hf isotope analyses, and whole-rock geochemistry of the Donggebi Mo deposit, eastern Tianshan, Northwest China, and their geological significance. *International Geology Review*, *57*, 446–462.

Zhang, H. R., Wei, G. F., Li, Y. J., Du, Z. G., & Cai, D. L. (2010). Carboniferous lithologic association and tectonic evolution of Dananhu arc in the East Tianshan Mountains. *Acta Petrologica et Mineralogica*, *29*, 1–14. (in Chinese with English abstract)

Zhang, L. C., Qin, K. Z., Ying, J. F., Xia, B., & Xu, J. S. (2004). The relationship between ore–forming processes and adakitic rock in Tuwu-Yandong porphyry copper metallogenic belt eastern Tianshan Mountains. *Acta Petrologica Sinica*, *20*, 259–268. (in Chinese with English abstract)

Zhang, L. C., Xiao, W. J., Qin, K. Z., & Zhang, Q. (2006). The adakite connection of the Tuwu-Yandong copper porphyry belt, eastern Tianshan, NW China: Trace element and Sr-Nd-Pb isotope geochemistry. *Mineralium Deposita*, *41*, 188–200.

Zhang, Y. Y., Yuan, C., Long, X. P., Sun, M., Huang, Z. Y., Du, L., & Wang, X. Y. (2017). Carboniferous bimodal volcanic rocks in the Eastern Tianshan, NW China: Evidence for arc rifting. *Gondwana Research*, *43*, 92–106.

Zhu, W. B., Ma, R. S., Guo, J. C., Sun, Y., Guo, L. Z., Xu, M. J., & Hu, D. Z. (2002). The coupling of sedimentary characteristics and tectonic development of Turpan-Hami basin and adjacent areas in Early Permian. *Geological Journal of China Universities*, *8*, 160–168. (in Chinese with English abstract)

How to cite this article: Sun X, Luan Y, Tang H, Tan X. Petrogenesis of rhyolite at Kalatage in the Eastern Tianshan, Northwest China: Evidences from geochemistry, zircon U–Pb geochronology, and Hf isotopes. *Geological Journal*. 2018;1–11. https://doi.org/10.1002/gj.3175